AGU PUBLICATIONS

JGR

Journal of Geophysical Research: Atmospheres

RESEARCH ARTICLE

10.1002/2017JD027968

Key Points:
- The directional absorption of mountain waves in the Northern Hemisphere is assessed using the ERA-Interim reanalysis between 2011 and 2016
- In the lower (middle to high) latitudes, the directional absorption of mountain waves mainly occurs in the troposphere (stratosphere)
- Directional absorption tends to suppress (enhance) the mountain wave drag in the lower (upper) stratosphere, especially in winter

Correspondence to:
Y. Wang,
yuanasm@nju.edu.cn

Citation:
Xu, X., Tang, Y., Wang, Y., & Xue, M. (2018). Directional absorption of parameterized mountain waves and its influence on the wave momentum transport in the Northern Hemisphere. *Journal of Geophysical Research: Atmospheres*, *123*, 2640–2654. https://doi.org/10.1002/2017JD027968

Received 30 OCT 2017
Accepted 17 JAN 2018
Accepted article online 23 JAN 2018
Published online 12 MAR 2018

Directional Absorption of Parameterized Mountain Waves and Its Influence on the Wave Momentum Transport in the Northern Hemisphere

Xin Xu[1,2], Ying Tang[1], Yuan Wang[1], and Ming Xue[1,3]

[1]Key Laboratory of Mesoscale Severe Weather/Ministry of Education, School of Atmospheric Sciences, Nanjing University, Nanjing, China, [2]State Key Laboratory of Severe Weather, Chinese Academy of Meteorological Sciences, Beijing, China, [3]Center for Analysis and Prediction of Storms, University of Oklahoma, Norman, OK, USA

Abstract The directional absorption of mountain waves in the Northern Hemisphere is assessed by examination of horizontal wind rotation using the 2.5° × 2.5° European Centre for Medium-Range Weather Forecasts ERA-Interim reanalysis between 2011 and 2016. In the deep layer of troposphere and stratosphere, the horizontal wind rotates by more than 120° all over the Northern Hemisphere primary mountainous areas, with the rotation mainly occurring in the troposphere (stratosphere) of lower (middle to high) latitudes. The rotation of tropospheric wind increases markedly in summer over the Tibetan Plateau and Iranian Plateau, due to the influence of Asian summer monsoonal circulation. The influence of directional absorption of mountain waves on the mountain wave momentum transport is also studied using a new parameterization scheme of orographic gravity wave drag (OGWD) which accounts for the effect of directional wind shear. Owing to the directional absorption, the wave momentum flux is attenuated by more than 50% in the troposphere of lower latitudes, producing considerable orographic gravity wave lift which is normal to the mean wind. Compared with the OGWD produced in traditional schemes assuming a unidirectional wind profile, the OGWD in the new scheme is suppressed in the lower stratosphere but enhanced in the upper stratosphere and lower mesosphere. This is because the directional absorption of mountain waves in the troposphere reduces the wave amplitude in the stratosphere. Consequently, mountain waves are prone to break at higher altitudes, which favors the production of stronger OGWD given the decrease of air density with height.

1. Introduction

The interaction between stably stratified airflow and mountains can generate upward propagating internal gravity waves. These waves, known as orographic gravity waves (OGWs) or mountain waves, are able to transport momentum and energy from their source regions to the middle atmosphere. It has been broadly recognized that OGWs play an important role in driving the atmospheric general circulation (Alexander et al., 2010; Fritts & Alexander, 2003; Holton, 1983), such as the Brewer-Dobson circulation in the mesosphere (Butchart, 2014).

In order to affect the general circulation in the middle atmosphere, mountain waves have to propagate into the stratosphere and/or mesosphere. In June and July 2014, a field campaign named "Deep propagating gravity waves experiment (DEEPWAVE)" was conducted in New Zealand, that is, a hot spot region of gravity waves in Austral winter (Eckermann & Preusse, 1999). One goal of DEEPWAVE is to understand the deep propagation of mountain waves from troposphere into the mesosphere and lower thermosphere (Fritts et al., 2016).

Several mechanisms have been found to affect the upward propagation of gravity waves, such as wave breaking. In general, the wave amplitude increases with height due to the decrease of density. Yet the waves cannot grow indefinitely; they will break up once they become saturated. Kaifler et al. (2015) examined the influence of source conditions on the penetration of mountain waves into the middle atmosphere by using the ground-based Rayleigh lidar observations in the DEEPWAVE experiment. Mesospheric gravity waves were mainly observed in the case of low-to-moderate lower tropospheric winds. By contrast, large-amplitude mountain waves forced by strong tropospheric winds tend to break in the stratosphere. Kruse et al. (2016) also found that mountain waves in New Zealand were frequently attenuated in a weak wind layer between z = 15 and 25 km (i.e., the lower stratosphere) above the subtropical jet. This layer was termed "valve layer" since it controlled the mountain wave momentum flux (WMF) through it. However, a more recent case study of DEEPWAVE by Bramberger et al. (2017) found that large-amplitude gravity waves can also be generated by strong tropospheric forcing.

The upward propagation of mountain waves is also affected by refraction and reflection. Dunkerton (1984) studied the propagation of stationary inertia gravity waves in the stratosphere by means of ray tracing. Owing to the horizontal shear of mean zonal wind, gravity waves were refracted and focused into the polar night jet, which was confirmed by recent observational and numerical studies (e.g., Ehard et al., 2017; Sato et al., 2009). Moreover, upgoing gravity waves can be reflected downward at the interface of static stability and/or wind shear discontinuities (e.g., Klemp & Lilly, 1975; Teixeira et al., 2008). Smith et al. (2008) examined the influence of tropopause on mountain waves entering the stratosphere. The abrupt change of temperature lapse rate across the tropopause makes it a preferable location for the occurrence of wave reflection.

In addition to wave breaking, refraction, and reflection, selective critical-level absorption by directional wind shear (Shutts, 1995) can influence the deep propagation of mountain waves as well. In theory, the wave components perpendicular to the horizontal wind will be advected downstream and finally form a turbulent wake (e.g., Guarino et al., 2016; Shutts, 1998; Xu, Song, et al., 2017). Therefore, the change of horizontal wind direction can result in a continuous absorption of mountain waves (Broad, 1995). The more the horizontal wind rotates with height, the more the waves are absorbed. Particularly, if the horizontal wind rotates by 180° (i.e., the wind direction is reversed), mountain waves will be totally absorbed and prevented from propagating beyond the wind reversal. The directional absorption of mountain waves has been documented in earlier studies, for example, Whiteway and Duck (1996) which investigated the mountain wave activities in the Canadian High Arctic using radiosonde measurements.

There are progressively more studies focusing on the directional absorption of mountain waves (e.g., Alexander et al., 2017; Broutman et al., 2017; Doyle & Jiang, 2006; Eckermann et al., 2007, 2016; Teixeira & Miranda, 2009; Teixeira & Yu, 2014; Xu et al., 2012, 2013). In the present work, the directional absorption of mountain waves in the Northern Hemisphere will be assessed using multiyear reanalysis which has not been reported in previous studies. Furthermore, the directional absorption of mountain waves produces a vertical divergence of WMF (which represents the body force exerted on the mean flow by gravity waves) *perpendicular* to the horizontal wind (Broad, 1995). This body force is named lift force (Xu et al., 2012), or *orographic gravity wave lift* (OGWL), which differs distinctively from the well-known *orographic gravity wave drag* (OGWD) that is parallel and opposed to the horizontal wind (e.g., Kim et al., 2003). For the parameterization of subgrid-scale OGWs in general circulation models, however, current operational schemes commonly assume a unidirectional wind profile, with the directional wind shear omitted. Therefore, the influence of directional absorption on the mountain wave momentum transport is still not well understood.

Xu, Wang, et al. (2017) recently developed a new OGWD parameterization scheme (hereafter the X17 scheme) based on the Gaussian beam approximation (GBA) (see Pulido & Rodas, 2011, hereafter PR11). This new scheme was used to study the impact of horizontal propagation on the mountain wave drag in the Northern Hemisphere (Xu, Shu, & Wang, 2017). As in this work, it will be modified to account for the effect of directional wind shear. With this modified X17 scheme, we are interested in exploring the impact of directional absorption on the momentum transport of mountain waves in the Northern Hemisphere.

The rest of this paper is organized as follows. In section 2 the data set and the GBA-based parameterization scheme are briefly described. Section 3 presents the main results including the features of wind rotation in the Northern Hemisphere, and the WMF, OGWL, and OGWD related to the momentum transport of mountain waves. Finally, the paper is summarized and discussed in section 4.

2. Data and Method

2.1. Terrain and Meteorological Data Sets

This work uses high-resolution (1 arc min, high as compared to the meteorological data set) terrain data, that is, the Global Relief Model (ETOPO1) developed at National Centers for Environmental Information of National Oceanic and Atmospheric Administration (Amante & Eakins, 2009). Also used are the daily, 2.5° ERA-Interim reanalyses in the period of 2011–2016, produced by the integrated forecast system of the European Centre for Medium-Range Weather Forecasts (ECMWF) (Dee et al., 2011). The integrated forecast system

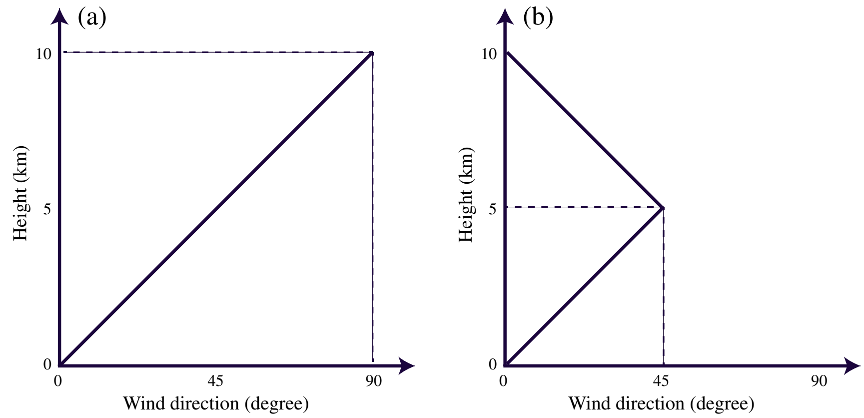

Figure 1. Schematic of effective wind rotation. (a) Horizontal wind veers uniformly with height from southward to westward, and (b) horizontal wind first veers with height from southward to southwestward then back to southward.

model has 60 levels, with the uppermost level placed at 0.1 hPa. Because we are more interested in gravity waves forced by mesoscale mountains larger than O (10) km, the 1 arc min terrain is resampled to a coarser resolution of 5 arc min. As a result, there are 31 × 31 terrain points within each of the 2.5° × 2.5° reanalysis grid cell.

2.2. Effective Rotation of Horizontal Wind With Height

The directional absorption of mountain waves is proportional to the rotation of horizontal wind with height. It is thus natural to use the wind rotation to assess the directional absorption of mountain waves. For idealized wind profiles that back or veer uniformly with height, it is easy to obtain the wind rotation (Figure 1a). But the realistic wind may turn with height very differently. Figure 1b illustrates such an example. The horizontal wind veers with height by 45° at $z = 5$ km, then backs to its surface direction at $z = 10$ km. Between $z = 5$ and 10 km, there is virtually no directional absorption, because the waves normal to the intervening wind have already been absorbed between $z = 0$ and 5 km. The *effective* wind rotation related to directional absorption is 45° at $z = 10$ km, although the wind vector actually undergoes a rotation of 90°. Hereafter, the term "wind rotation" will denote "effective wind rotation" unless otherwise stated.

In the calculation of wind rotation, surface wind is defined as the horizontal wind at the first model level above the maximum subgrid-scale orography (SSO) in each of the 2.5° grid cell (Figure 2a). Wind rotations

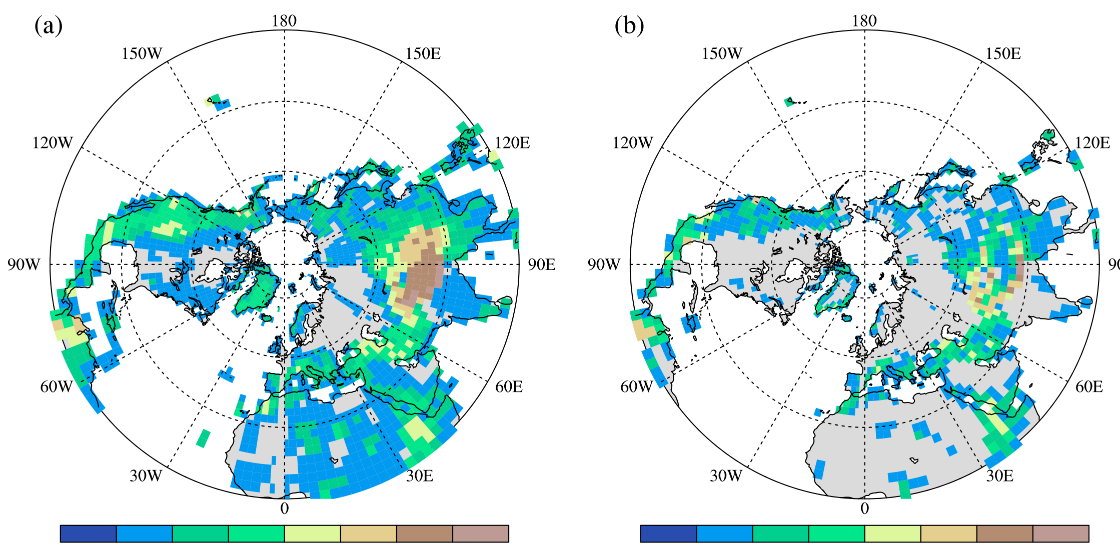

Figure 2. (a) Maximum and (b) standard deviation of SSO (unit: meter) within the 2.5° ECMWF ERA-Interim reanalysis grids in the Northern Hemisphere. Values shown in (a) and (b) are larger than 500 m and 200 m, respectively.

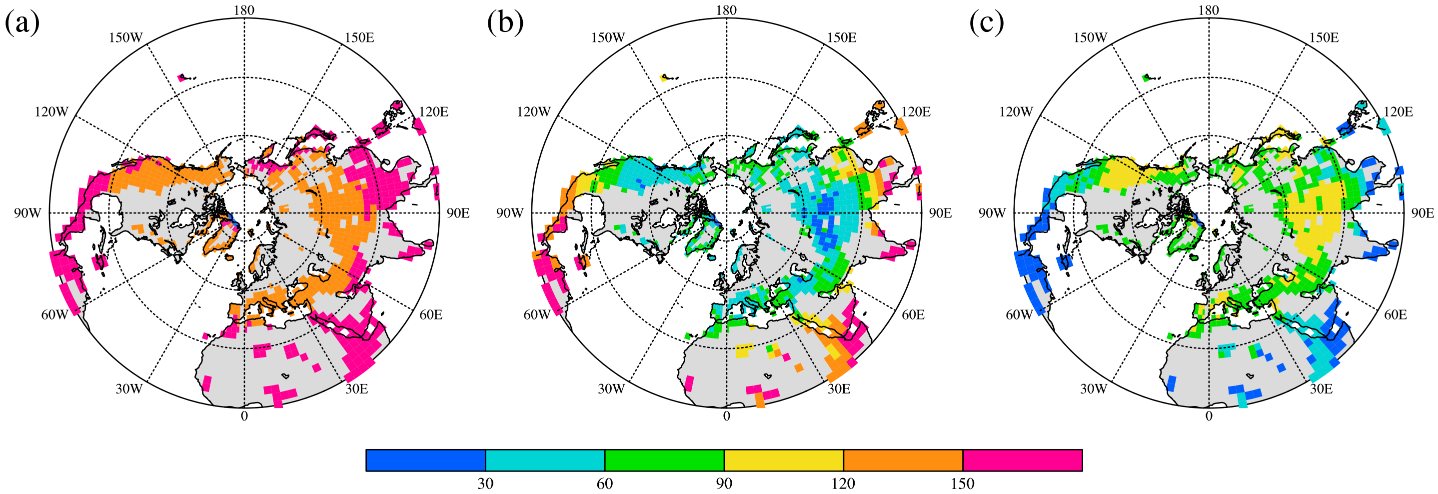

Figure 3. Annual mean wind rotation (unit: degree) in the (a) deep layer of troposphere and stratosphere, (b) troposphere, and (c) stratosphere of Northern Hemisphere averaged between 2011 and 2016. The wind rotation is only shown in the mountainous areas where the standard deviation of SSO exceeds 200 m.

at the tropopause and stratopause are separately calculated. The former one denotes the rotation of horizontal wind in the troposphere, whereas the latter measures the wind rotation in the deep layer of troposphere and stratosphere. Their difference thus gives the wind rotation in the stratosphere. The tropopause is defined at the level of 2 PVU in the Northern Hemisphere which is provided by the ECMWF ERA-Interim reanalysis. But this is not the case for stratopause, which is defined at the 1 hPa pressure level (around z = 50 km) for simplicity.

2.3. Modified X17 Scheme

The X17 scheme developed in Xu, Wang, et al. (2017) is based on a higher-order ray method, that is, the GBA. Gravity waves are well defined even at ray caustics where multiple rays intersect (PR11). In the X17 scheme the ambient wind is assumed to be unidirectional, which needs to be revised herein to take into account the directional absorption of mountain waves.

Operational OGWD parameterization schemes usually assume hydrostatic gravity waves, with the Earth's rotation neglected (e.g., Lott & Miller, 1997, hereafter LM97). Under the first-order Wentzel-Kramers-Brillouin (WKB) approximation, the perturbed vertical velocity in the spectral space is given by (see equation (25) of Teixeira et al. (2004))

$$\hat{w}(k,l,z) = \hat{w}(k,l,z=0)\left[\frac{m_0(z=0)}{m_0(z)}\right]^{1/2} \exp\left[i\int_0^z m_0(\xi)\mathrm{d}\xi\right], \tag{1}$$

where $m_0(z) = \frac{N(z)\sqrt{k^2+l^2}}{U(z)k+V(z)l}$ is the vertical wave number, $N(z)$ is the Brunt-Väisälä frequency, $\mathbf{K} = (k, l)$ is the horizontal wave number vector, and $\mathbf{V}(z) = (U(z), V(z))$ is the horizontally uniform base state wind. The vertical wave number has the same form as in the case of constant wind and buoyancy frequency (e.g., Smith, 1980), although they actually depend on z. The directional wind shear usually produces a nontrivial wind vertical curvature. However, under the first-order WKB approximation, the effect of wind vertical curvature can be omitted because it only contributes to the second-order WKB solution (see equation (24) of Teixeira et al. (2004)).

As in the original X17 scheme, the modified X17 scheme first calculates the WMF at the reference level z_0,

$$\boldsymbol{\tau}_\mathbf{0} = \boldsymbol{\tau}(z_0) = -\overline{\rho}_0\overline{\mathbf{v}_{\boldsymbol{h}}^{'}w^{'}}, \tag{2}$$

where $\overline{\rho}_0$ is the base state density at the reference level and $\mathbf{v}_{\boldsymbol{h}}^{'}$ and $w^{'}$ are the perturbed horizontal and vertical velocities, with overbar denoting the areal mean within the 2.5° reanalysis grid cell. The reference level is determined by the low-level mean wind and stratification and the standard deviation of SSO (Figure 2b), which was detailed in LM97. The perturbed velocities are obtained via superposition of

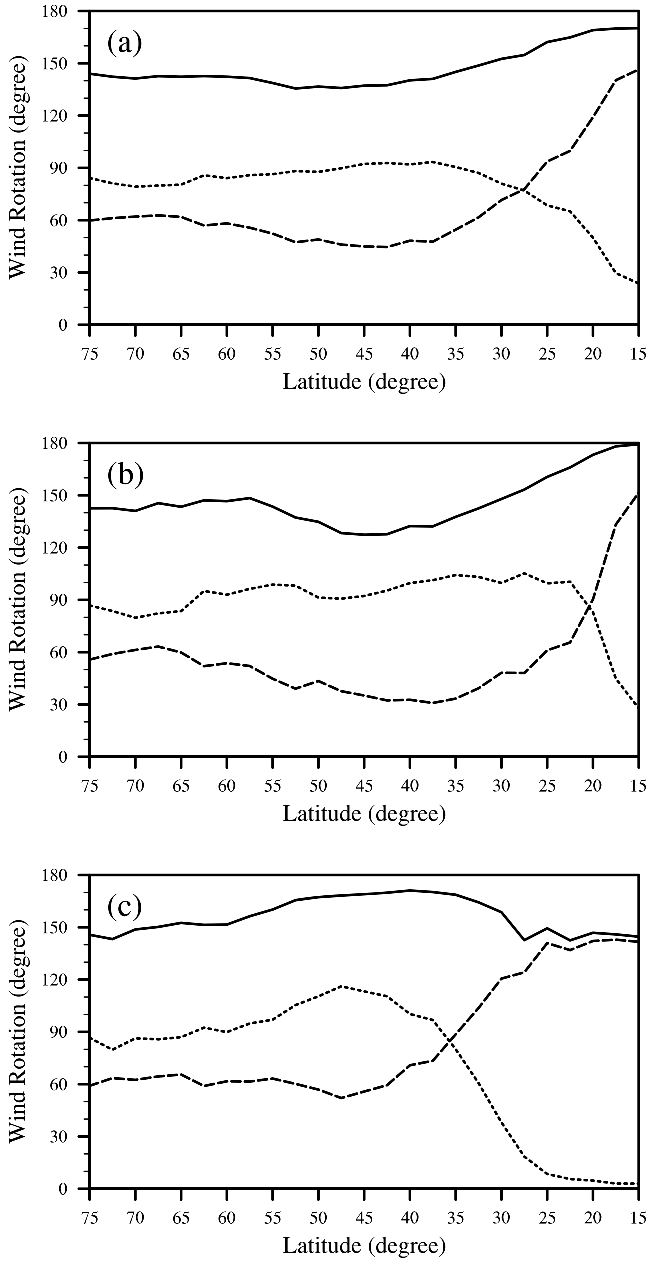

Figure 4. Zonal mean wind rotation (unit: degree) in the Northern Hemisphere averaged between 2011 and 2016. (a) Annual, (b) January, and (c) July. Solid lines are the wind rotation in the deep layer of troposphere and stratosphere, whereas dashed and dotted lines denote the wind rotations in the troposphere and stratosphere, respectively.

20×20 Gaussians, with a spectral resolution of $2\pi/2.5°$. Readers are referred to PR11 and Xu, Wang, et al. (2017) for more details about the GBA solution.

The WMF is propagated upward level by level. Supposing there are n levels above the reference level, that is, $L_1, L_2, L_3, \ldots L_n$, at level L_i, unlike the X17 scheme, we first detect the wind rotation between L_{i-1} and L_i and remove the WMF associated with the wave components normal to the intervening winds. The selectively removed WMF is perpendicular to the mean wind, that is, OGWL. Afterward, the maximum wave amplitude (η_m) is computed in accordance with the GBA solution and compared with the saturation wave amplitude (η_{sat}). Note that the waves removed below L_i should be discarded in the calculation of η_m. The saturation wave amplitude is derived using the criterion of dynamic instability, that is, $Ri < 0.25$ (Palmer et al., 1986), which is given as follows (cf. equation (23) of Xu, Wang, et al., 2017)

$$\eta_{\text{sat}}(z) = \frac{U(z)}{N(z)}\overline{Ri}^{-1/2}\left(1 + 2\overline{Ri}^{1/2}\right)\left\{2\overline{Ri}^{1/4}\left(1 + 2\overline{Ri}^{1/2}\right)^{-1/2} - 1\right\}, \quad (3)$$

with $\overline{Ri}$ being the mean flow Richardson number. (It is worth noting that this saturated wave amplitude is derived according to the two-dimensional gravity wave theory which considers only one wave number harmonic. Yet it was widely used in the parameterization of OGWD because it is difficult to obtain the analytical expression of saturated wave amplitude for three-dimensional gravity waves.) In the case of $\eta_{\text{sat}} > \eta_m$, the WMF is simply passed to the next level without attenuation; otherwise, mountain waves are supposed to break and produce a vertical divergence of WMF known as OGWD. Consequently, the WMF is scaled by a factor of $(\eta_{\text{sat}}/\eta_m)^2$ before passing to the next level.

In short, for mountain waves generated in directional shear winds, they can produce not only OGWD but also OGWL, both of which are calculated as follows

$$\mathbf{F}_{\text{GW}} = \frac{\partial \overline{\mathbf{V}}}{\partial t} = \frac{1}{\overline{\rho}(z)}\frac{\partial \boldsymbol{\tau}}{\partial z} = \frac{1}{\overline{\rho}(z)}\frac{\partial}{\partial z}\left[-\overline{\rho}(z)\overline{\mathbf{v}_h' w'}\right], \quad (4)$$

where $\overline{\rho}(z)$ is the base state density at height z.

3. Results

3.1. Wind Rotation

Figure 3 presents the geographical distribution of annual mean wind rotation averaged between 2011 and 2016. Note that in this study we only consider the mountainous areas where the standard deviation of SSO is greater than 200 m unless otherwise stated. In the deep layer of troposphere and stratosphere (Figure 3a), large wind rotations (>120°) are found all over the mountainous areas under consideration, especially in the lower latitudes south of about 30°N, such as East and Southeast Asia, East Africa, and central North America. These are the well-known monsoonal regions. The large wind rotations suggest that even in the absence of wave breaking caused by wave saturation, mountain waves will be significantly prevented from penetrating into the mesosphere. The horizontal wind in the troposphere (Figure 3b) rotates by less than 90° in the middle to high latitudes, which is as low as 30° over central Asia. On the contrary, the stratospheric wind rotates more notably in the middle to high than in the lower latitudes (Figure 3c). This is clearly shown in Figure 4a, which depicts the zonal mean wind rotation. South of 30°N, the horizontal wind rotation mainly takes place in the troposphere (over 90°); poleward, the stratospheric wind experiences greater rotation than its tropospheric counterpart.

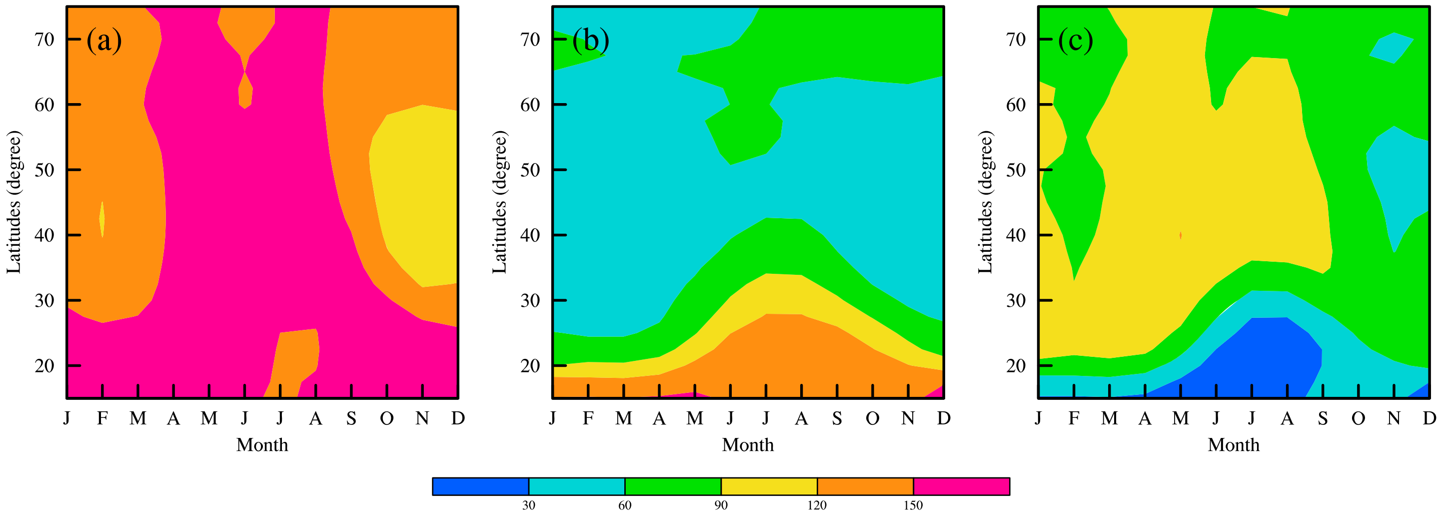

Figure 5. Monthly variation of zonal mean wind rotation (unit: degree) in the (a) deep layer of troposphere and stratosphere, (b) troposphere, and (c) stratosphere of Northern Hemisphere averaged between 2011 and 2016.

Figure 5 illustrates the monthly variation of zonal mean wind rotation in the Northern Hemisphere. In the deep layer of troposphere and stratosphere (Figure 5a), there is little monthly variation in the lower latitudes south of 30°N. In the middle to high latitudes, the horizontal wind rotates by smaller degrees from August to March, especially between 30°N and 60°N from September to December. In the troposphere (Figure 5b), the large wind rotations found in the lower latitudes move poleward from April, reaching their northernmost position in July; afterward, they retrogress southward until December. In the high latitudes a persistent enhancement of wind rotation emerges from June to December. In the stratosphere (Figure 5c), the small wind rotations occurring in the lower latitudes expand northward from April, reaching about 30°N in July, which then moves southward until December. It is also found that the wind in middle to high latitudes rotate more notably between May and September.

The geographical distributions of wind rotation in January and July are shown in Figure 6, with their zonal mean given in Figures 4b and 4c, respectively. In January (Figures 6a–6c), the spatial patterns of wind rotation are quite similar to the annual mean (Figure 3). In July, the rotation of tropospheric wind (Figure 6e) nearly increases all over the mountainous areas under consideration except in the lower latitudes south of about 20°N. The most notable increases occur over the Tibetan and Iranian Plateaus (Figure 6h), which will be investigated next. In the middle to high latitudes, the reduced wind rotation found in the wintertime is ascribed to the occurrence of a polar vortex, with two centers located in North America and East Asia, respectively (not shown). The vertically coherent northwesterlies associated with the deep polar vortex produces smaller directional wind shear over the mountainous areas of middle to high latitudes. Conversely, the stratospheric wind undergoes smaller rotations in middle to lower latitudes (Figures 6f and 6i). Overall, in the deep layer of troposphere and stratosphere, it is featured by increased (decreased) wind rotation north (south) of about 30° in July than in January (Figure 6g).

What causes the notable monthly variations of wind rotation over the Tibetan and Iranian Plateaus? Figure 7 compares the horizontal winds in January and July averaged between 2011 and 2016. We are more interested in the rotation of *tropospheric wind*, because the directional absorption of mountain waves at lower levels will influence their propagation at upper levels. In January (Figures 7a, 7c, and 7e), the tropospheric winds are predominantly westerlies in midlatitudes. Hence, there is little wind rotation (less than 30°) over the Tibetan and Iranian Plateaus. In July, the 700 hPa wind (Figure 7b) exhibits a synoptic-scale anticyclone over the Iranian Plateau. (Seen from Figure 2a, the Iranian Plateau is about 3,000 m high, i.e., near 700 hPa.) Higher at 500 hPa (Figure 7d), the anticyclone center shifts to the Arabian Peninsula and East Africa, with the northern/southern part of the Iranian Plateau dominated by northwesterlies/northeasterlies. At even higher level of 200 hPa that is close to the tropopause (Figure 7f), the Iranian Plateau is under the influence of the

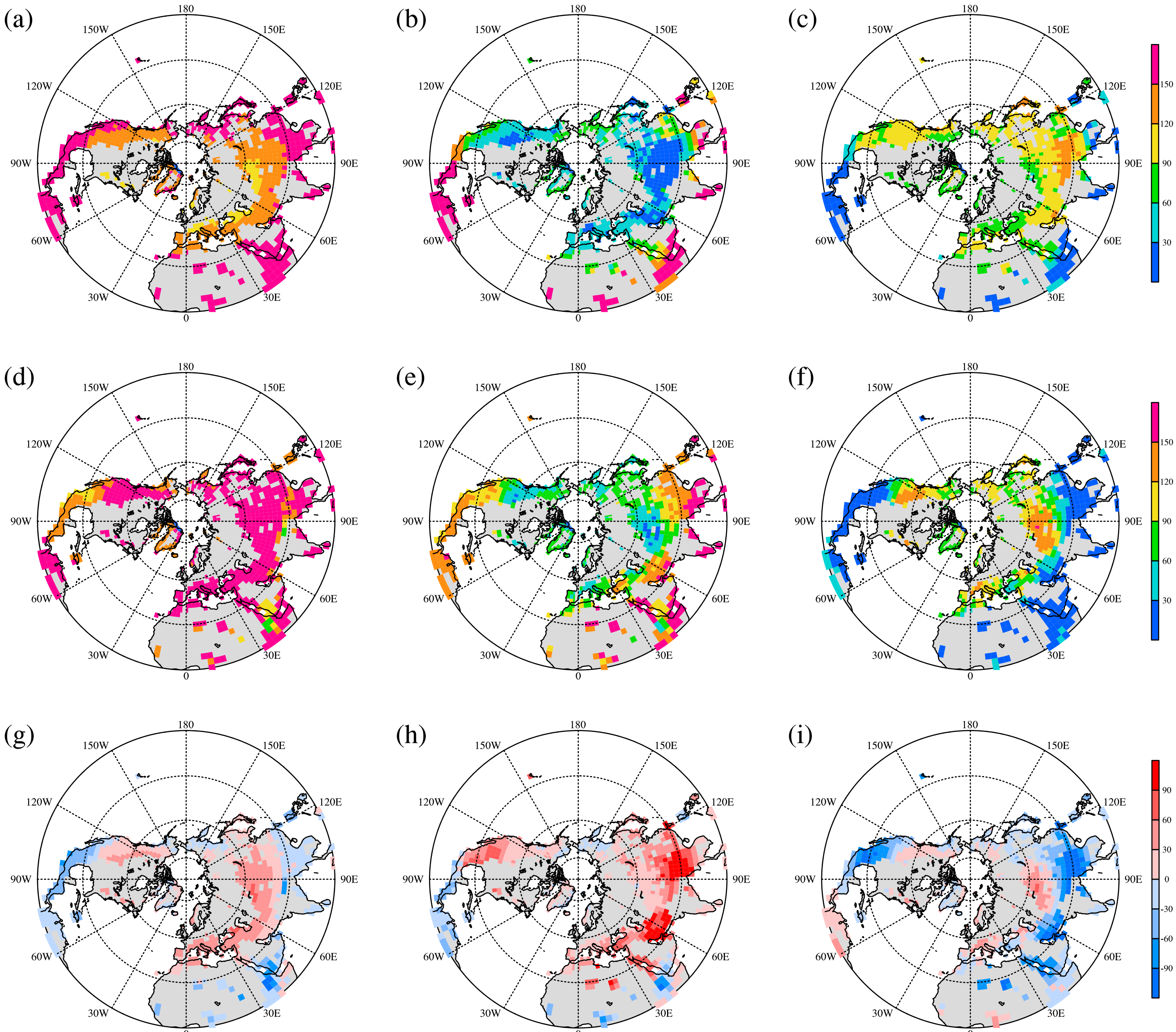

Figure 6. Same as Figure 3 but in January (a–c) and July (d–f). (g–i) are the differences between the wind rotations in January and July (July minus January).

planetary-scale South Asia High (SAH), with westerlies (easterlies) prevailing over its northern (southern) part. Close examination shows that the tropospheric wind generally backs/veers with height over the northern/southern Iranian Plateau.

The Tibetan Plateau has a much greater spatial coverage in the middle to lower latitudes. The 500 hPa and 200 hPa winds are consistently eastward north of 30°N (Figures 7d and 7f). (The 500 hPa level is just above the Tibetan Plateau; see Figure 2a.) In consequence, there are virtually small wind rotations over the western and northern Tibetan Plateau (Figure 6e). In the southwestern and southern Tibetan Plateau, southeasterlies and southerlies are found at 500 hPa in association with the cyclonic circulation centered at the South Asian subcontinent. The southeastern Tibetan Plateau is influenced by southwesterlies associated with the northwestern Pacific subtropic high. At 200 hPa, the SAH center is directly above the Tibetan Plateau, thus giving

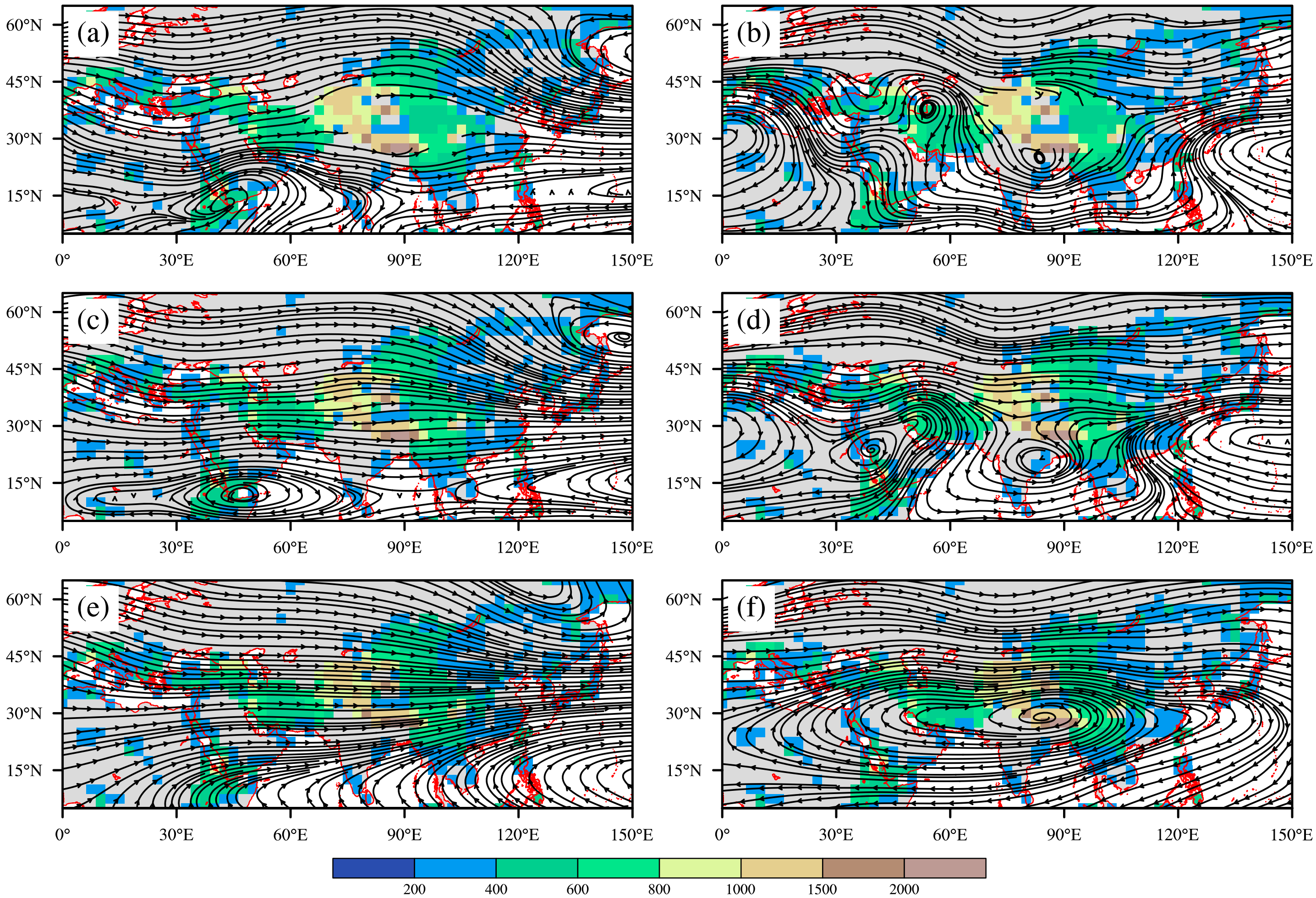

Figure 7. Monthly mean horizontal wind in January (left column) and July (right column) at (a, b) 700 hPa, (c, d) 500 hPa, and (e, f) 200 hPa averaged between 2011 and 2016. The standard deviation of SSO is shaded (unit: meter).

rise to westerlies/easterlies in its northern/southern part (Figure 7f). In view of these upper-level and low-level flow patterns, the horizontal wind rotates markedly over the southern Tibetan Plateau (Figure 6e).

3.2. Variation of WMF With Height

Figure 8 shows the vertical distribution of zonal mean WMF averaged between 2011 and 2016 by using the modified X17 scheme which includes the directional absorption of mountain waves. In January (Figure 8a), the WMF is decreased by more than 50% in the troposphere of lower latitudes (south of about 20°N), with the largest decrease in excess of 80%. By contrast, there is little decrease (<10%) between about 35°N and 55°N, while a moderate decrease of up to 20% is commonly seen in the high latitudes. This agrees well with the latitudinal variation of wind rotation (Figure 4b), implying the importance of directional absorption in reducing the WMF in the troposphere. Indeed, there is little OGWD but considerable OGWL in the troposphere of lower latitudes, as will be shown later. In the stratosphere, the WMF keeps decreasing with height. The most salient decrease occurs at about $z = 20$ km between 20°N and 40°N. Given the relatively small wind rotations at these latitudes, this rapid falloff of WMF is due mainly to the breaking of mountain waves, as revealed by the localized OGWD maxima in the valve layer of lower stratosphere (see section 3.3). The height decay of the WMF slows down in the middle and upper stratosphere. On average, only a small fraction of WMF (less than 20%) can be transported to the mesosphere. However, in the wintertime over 20% of the WMF is transported into the mesosphere at midlatitudes near 45–50°N, suggesting that the polar night jet is able to transit gravity waves to higher altitudes.

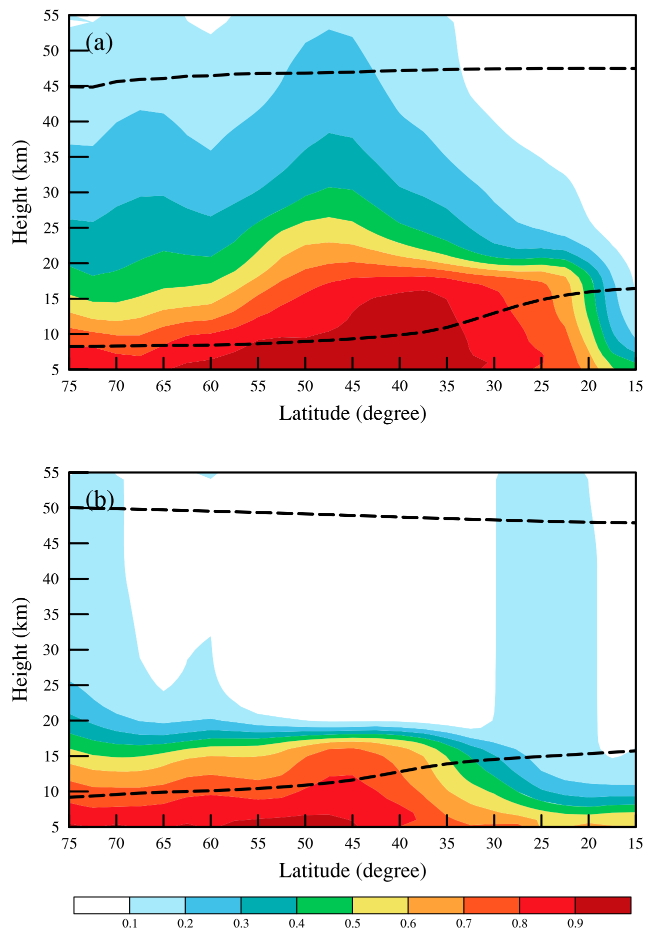

Figure 8. Height variation of normalized wave momentum flux in (a) January and (b) July averaged between 2011 and 2016 in the Northern Hemisphere. The normalization is made with respect to the wave momentum flux at the reference level.

In July (Figure 8b), there is larger decrease of WMF in the troposphere than in January. The enhanced attenuation of WMF is attributed to the increase of tropospheric wind rotation (Figure 4c). In the stratosphere, the WMF also decays rapidly around z = 20 km, resulting in a sharp vertical gradient. Unlike in January, nearly all the WMFs are absorbed in the lower stratosphere between 30°N and 65°N. This is owing to the occurrence of a hemisphere-scale *wind reversal* in the lower stratosphere, as depicted in Figure 7b of Xu, Shu, and Wang (2017). (The presence of the wind reversal can be inferred from the nearly 180° wind rotation in the midlatitudes shown in Figure 4c.) On the contrary, there are two narrow windows for mountain waves in the high and lower latitudes, with 10%–20% of the WMF leaking into the mesosphere.

3.3. Distribution of OGWL

The zonal mean OGWL averaged between 2011 and 2016 is shown in Figure 9. In January (Figure 9a), the OGWL is found up to the lower mesosphere except south of ~20°N where the wind turns by almost 180° (Figure 4b), indicating total absorption. The magnitude of OGWL in general increases with height, despite the small vertical gradients of WMF at high altitudes (Figure 8a). According to equation (4), this large OGWL in the upper levels must be attributed to the height decrease of air density. In July (Figure 9b), in the lower latitudes south of about 25°N, the OGWL is confined in the troposphere, as a consequence of little wind rotation in the stratosphere (Figure 4c). Northward, the OGWL is observed in both the troposphere and lower stratosphere, peaking at about z = 20 km. The stratospheric OGWL appears to slope upward with latitude, coincident with the hemisphere-scale wind reversal found in the summer stratosphere (see Figure 7b of Xu, Shu, and Wang, 2017).

3.4. Influence on OGWD

As noticed in section 2.3, both OGWL and OGWD can be produced by mountain waves generated in directional shear winds. To better understand the influence of directional absorption, here we consider two more sets of OGWD, in addition to the OGWD obtained from the modified X17 scheme. One is obtained from the LM97 scheme; that is, neither the horizontal propagation nor the directional absorption of mountain waves is considered. The other set uses the X17 scheme as in Xu, Shu, and Wang (2017) which incorporates the horizontal propagation of mountain waves but with no directional absorption. It should be emphasized that the OGWD under investigation are obtained using offline parametrization schemes, which are not supposed to be the same as in reality, or those produced by the state-of-the-art numerical weather prediction models. It is also noteworthy that the complete LM97 scheme considers not only the gravity wave drag owing to vertically propagating mountain waves but also the orographic drag caused by low-level flow blocking. Here we only use the gravity wave drag component of the LM97 scheme. Furthermore, in the LM97 scheme the real terrain is fitted to idealized elliptical orography according to their statistic features. Then the WMF at the reference level is calculated according to the analytical expression of mountain wave drag derived in Phillips (1984). This differs from the X17 scheme which calculates the reference-level WMF using the GBA solution. In order to make these two schemes comparable, the reference-level WMF in the LM97 scheme is set to that in the X17 scheme.

Figure 10 presents the three sets of OGWD averaged between 2011 and 2016, with their differences shown in Figure 11. Generally speaking, the three sets of OGWD show similar features. Taking the OGWD in January as an example, there is no OGWD in the lower latitudes south of about 20°N. A localized OGWD maximum is evident at about z = 20 km near 35°N. As shown in Figure 7a of Xu, Shu, and Wang (2017), the mean wind in the wintertime is relatively weak near this height, which is sandwiched by the tropospheric jet below and mesospheric jet above. The localized OGWD maxima mentioned above suggests that mountain waves are prone to break in this weak wind layer and deposit wave momentum into the mean flow. This stratospheric wind

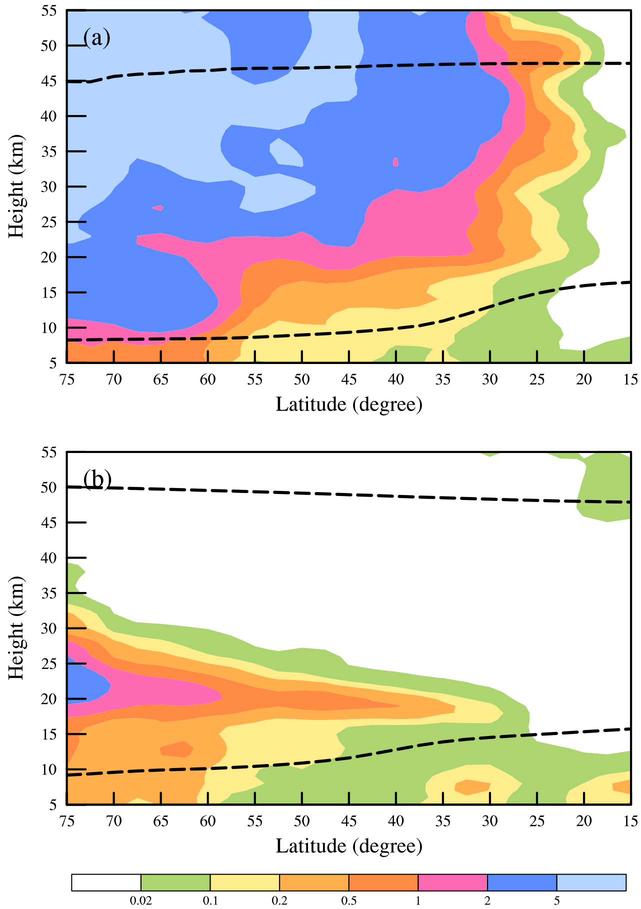

Figure 9. Vertical distribution of zonal mean orographic gravity wave lift (unit: 10^{-6} m s^{-2}) in (a) January and (b) July averaged between 2011 and 2016 in the Northern Hemisphere. The two dashed lines indicate the tropopause and stratopause, respectively.

minimum is thus called valve layer by Kruse et al. (2016). In the LM97 scheme mountain-wave breaking tends to take place at lower height (see the OGWD immediately above the tropopause in Figure 10a) than in the other two schemes (Figures 10c and 10e). This is attributed to the horizontal propagation of mountain waves which reduces the wave amplitude and pushes wave breaking to higher altitudes (Eckermann et al., 2015). For instance, the wintertime OGWD is suppressed (enhanced) in the lower stratosphere (middle to upper stratosphere and lower mesosphere) in the X17 scheme when compared to the LM97 scheme (Figure 11a), consistent with the results of Xu, Shu, and Wang (2017).

The valve layer OGWD in the modified X17 scheme occurs at slightly higher altitude than in the X17 scheme (Figures 10c and 10e). This is because the wave amplitude is reduced further by the directional absorption of mountain waves, leading to an even higher wave breaking level. Since mountain waves are directionally absorbed, transporting less wave momentum into the stratosphere, the valve layer OGWD in the modified X17 scheme is smaller than in the X17 scheme. In fact, the modified X17 scheme appears to produce weaker OGWD in nearly all the stratosphere (Figure 11e). As a result, the OGWD in the modified X17 scheme is suppressed even in the middle stratosphere north of about 45°N, as compared with the LM97 scheme (Figure 11c). Nonetheless, the OGWD is still enhanced in the upper stratosphere and lower mesosphere, as in the case of X17 scheme. This suggests that in the upper atmosphere the influence of directional absorption in causing the WMF reduction can be superseded by the decrease of air density with height.

The similarities between Figures 10c and 10e (as well as Figures 10d and 10f) do not mean that the effect of directional absorption of mountain waves can be replaced by that of horizontal propagation, or vice versa. The directional absorption of mountain waves can notably affect the momentum transport of mountain waves. For example, it causes a deposition of WMF by more than 50% in the troposphere of lower latitudes (Figure 8). In the middle atmosphere, these two sets of OGWD are found to differ a lot, especially in the middle to high latitudes, with the magnitude of differences of the same order of OGWD (Figures 10 and 11). Moreover, although not examined herein, the directional absorption of mountain waves can also affect the direction of OGWD. As pointed out in Teixeira et al. (2004) and Xu, Song et al. (2017), the WMF generated in directional shear wind is usually misaligned with the horizontal wind, even for mountain waves forced by axisymmetric orography. Consequently, the vertical divergence of WMF due to wave breaking is not parallel to the horizontal wind either. Strictly speaking, it may be improper to use the term "OGWD" which denotes a drag force antiparallel to the horizontal wind. This is beyond the scope of the present study.

4. Summary and Discussion

In an earlier study of Xu, Wang et al. (2017), a new parameterization scheme of OGWD was developed by using the GBA method (i.e., the X17 scheme), which was used to investigate the impact of horizontal propagation of mountain waves in the Northern Hemisphere (Xu, Shu, & Wang, 2017). As a third part of this series of papers, the X17 scheme is modified herein to allow for the *directional* wind shear. Then the modified X17 scheme is employed to address the directional absorption of mountain waves as well as its influence on the wave momentum transport in the Northern Hemisphere.

Using the 2.5° ERA-Interim reanalysis between 2011 and 2016, the directional absorption of mountain waves is assessed through the examination of horizontal wind rotation, because the more the horizontal wind rotates with height, the more the mountain waves are attenuated. It is found that the horizontal wind

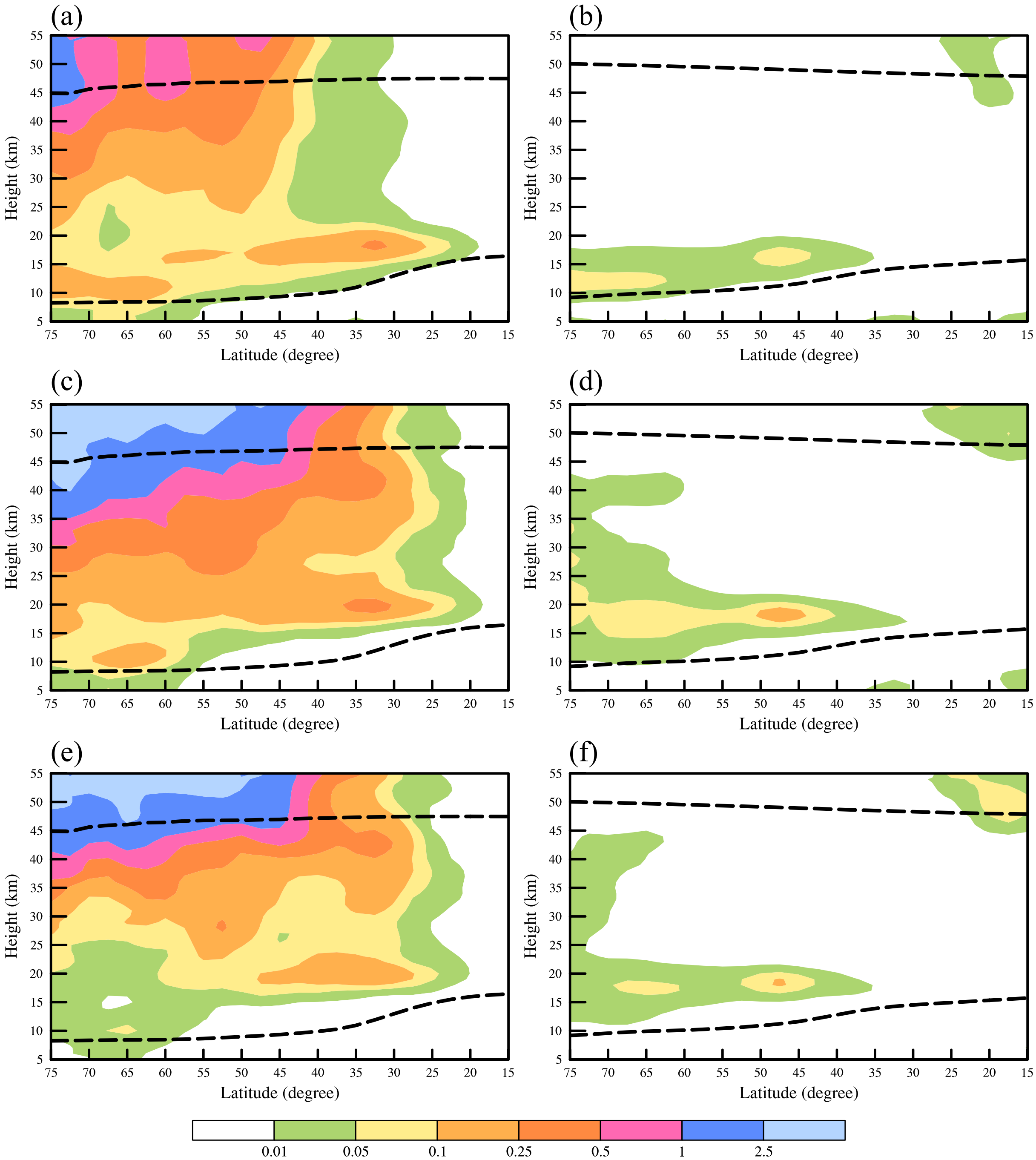

Figure 10. Vertical distribution of zonal mean orographic gravity wave drag (unit: 10^{-4} m s^{-2}) in January (left column) and July (right column) averaged between 2011 and 2016 in the Northern Hemisphere. (a, b) LM97 scheme, (c, d) X17 scheme, and (e, f) modified X17 scheme.

rotates by more than 120° in the deep layer of troposphere and stratosphere, especially in the lower-latitude monsoonal areas (e.g., East and Southeast Asia, East Africa, and central North America). South of about 30°N the wind rotation generally occurs in the troposphere, while the wind in the middle to high latitudes experiences greater rotations in the stratosphere.

The monthly variation of horizontal wind rotation is also examined. In the lower latitudes, the large wind rotations in the troposphere move northward from April to July, followed by southward retrogression until

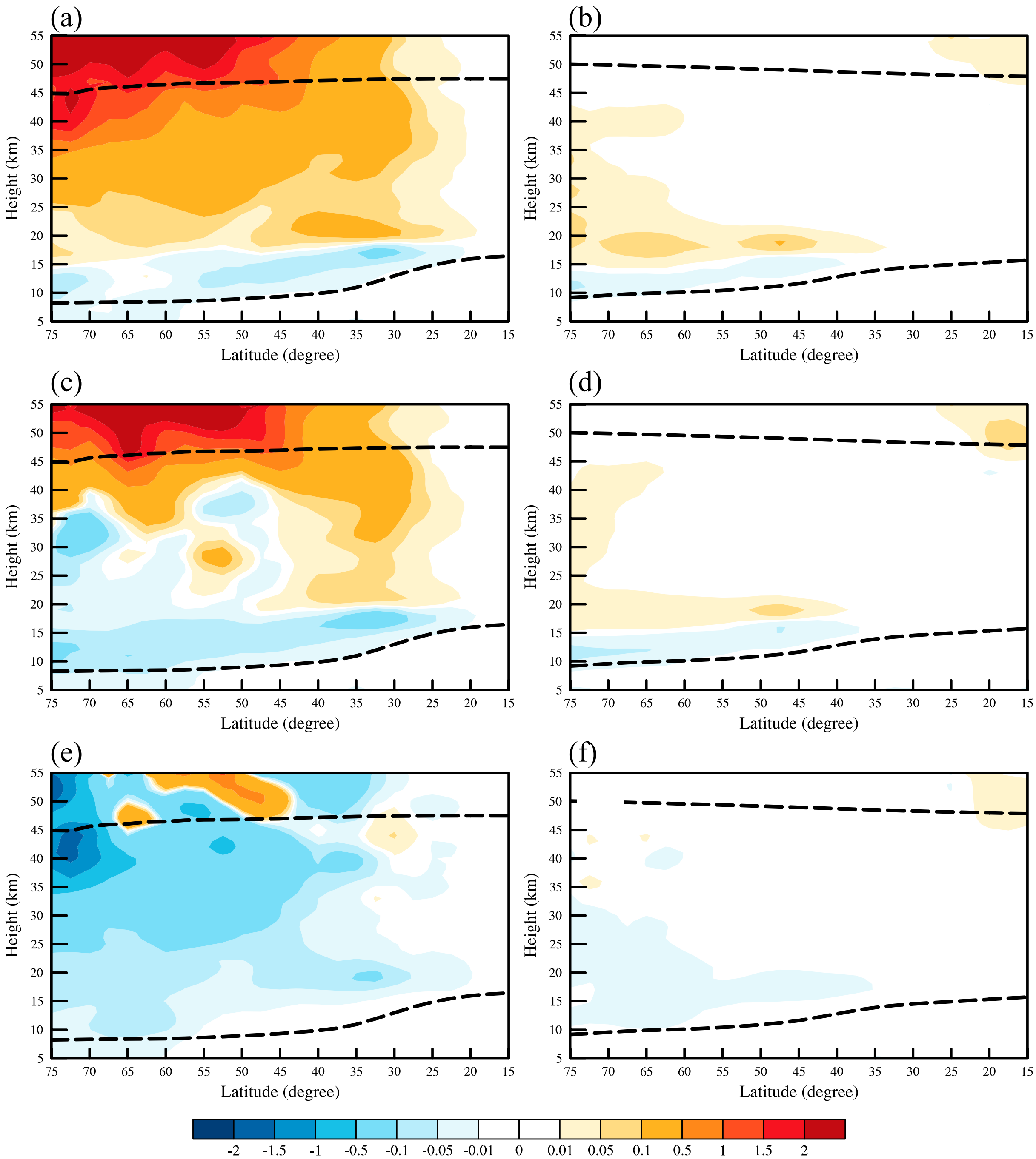

Figure 11. Difference between the zonal mean orographic gravity wave drag (unit: 10^{-4} m s^{-2}) in January (left column) and July (right column) averaged between 2011 and 2016 in the Northern Hemisphere. (a, b) X17 minus LM97, (c, d) modified X17 minus LM97, and (e, f) modified X17 minus X17.

December. Meanwhile, the small wind rotations in the stratosphere undergo similar northward-southward movement. Consequently, there is little monthly variation in the deep layer of troposphere and stratosphere. In the middle to high latitudes, the horizontal wind rotates by smaller degrees from August to March, especially between 30°N and 60°N, with the most notable decrease occurring in the stratosphere.

Particular interest is paid to the monthly variation of wind rotation in the troposphere. Compared with January, the wind rotation in July increases significantly around 30°N, especially over the Tibetan and

Iranian Plateaus. In January, westerlies prevail in the entire troposphere of midlatitudes, giving rise to small wind rotations. In July, the upper troposphere is dominated by the planetary-scale SAH over the Tibetan Plateau, with westerlies (easterlies) found north (south) of ~30°N. In the middle to lower troposphere, broad westerlies/southwesterlies are shown to extend from East Africa to Southeast Asia but change to southerlies/southeasterlies in East Asia due to the influence of the northwestern Pacific subtropic high. It is therefore the Asian summer monsoonal circulation that produces the large wind rotations observed in the troposphere of lower latitudes.

Under the influence of directional wind shear, the WMF is decreased by 50%–80% in the troposphere of lower latitudes, producing considerable OGWL that is normal to the mean flow. In contrast, the OGWD mainly occurs in the middle atmosphere. In January, it is found in both the stratosphere and mesosphere, with a localized center in the lower stratosphere valve layer. In July, the OGWD is confined in the lower stratosphere underneath the hemisphere-scale wind reversal. In general, the magnitude of OGWD is 2 orders larger than that of OGWL. However, this does not mean that the directional absorption of mountain waves and the resultant OGWL are unimportant. The directional absorption can help reduce the mountain wave amplitude which affects wave breaking and thus OGWD at higher altitudes.

To better understand the effect of directional absorption, the OGWD obtained from the modified X17 scheme is compared with two other sets of OGWD obtained from the LM97 and original X17 schemes, respectively. At least two effects of directional absorption are revealed. For one thing, it reduces the WMF transported into the stratosphere, tending to produce *smaller* OGWD. This is confirmed by the weaker OGWD in the modified X17 scheme than in the X17 scheme. For another, the mountain wave amplitude is decreased as a result of WMF attenuation. Hence, mountain waves are prone to break at higher altitudes, as evidenced by the highest valve layer OGWD maxima in the modified X17 scheme. Given the height decay of density, breaking of mountain waves at upper levels is favorable for the generation of *stronger* OGWD. For example, during the DEEPWAVE experiment mountain waves were found to break at about $z = 80$ km downstream of the Auckland Islands, producing a very large westward flow acceleration of about 350 m s^{-1} h^{-1} and dynamical heating of about 8 K h^{-1} which can greatly affect the local circulation (Eckermann et al., 2016). Therefore, the directional absorption of mountain waves appears to have two *opposite* effects on the OGWD. Nevertheless, when taking into account the directional absorption, the wintertime OGWD is enhanced in the upper stratosphere and lower mesosphere while suppressed in the lower stratosphere. This is in qualitative agreement with the findings of Xu, Shu, and Wang (2017), suggesting its potential use in alleviating the known problems of traditional OGWD parametrization schemes, that is, excessive OGWD in the lower stratosphere and insufficient gravity wave forcing in the mesosphere (Klinker & Sardeshmukh, 1992; Long et al., 2012).

To sum up, the directional absorption of mountain waves is able to redistribute the wave momentum between the troposphere and middle atmosphere. In the case of *unidirectional* wind, the WMF is primarily transported to the middle atmosphere, contributing more to the large-scale circulation. On the contrary for *directional* wind, the WMF can be significantly attenuated in the troposphere (especially in the lower latitudes), imposing a direct (and distinctively different, i.e., OGWL) influence on the short-term weather evolution (e.g., Martin & Lott, 2007). The current work and Xu, Shu, and Wang (2017) perform an *offline* evaluation of directional absorption and horizontal propagation of mountain waves by using the GBA-based parameterization scheme. In the future, the new scheme will be implemented in operational numerical weather prediction and climate models such that these two effects can be examined more accurately by running simulations with sophisticated physics and dynamical constraints. While the new scheme provides an opportunity of better describing the subgrid-scale mountain waves, it needs to be optimized before practical implementation in the model. Compared with the traditional schemes, the calculation of gravity wave amplitude (for the purpose of detecting wave breaking) using the GBA solution is time consuming, because it involves an integral of vertical wave number varying with height (see equation (21) of PR11). This can be partly solved by employing a relatively small number of Gaussians for the construction of mountain waves, though it may cause a degradation of the wave solution. Additionally, for the calculation of reference-level WMF, one may adopt the analytical formulae of mountain wave drag for elliptical mountains as in traditional parameterization schemes (e.g., the LM97 scheme) instead of the GBA solution, which can further reduce the computational cost. The implementation details and performance of the new parameterization scheme will be given in a separate paper.

Acknowledgments
This study is supported by the National Fundamental Research 973 Program of China (2015CB452801 and 2013CB430103) and the National Science Foundation of China (grant 41505046). Xin Xu is supported by the Fundamental Research Program of Chinese Academy of Meteorological Sciences (2017Z017 and grant 2017LASW-A02) as well. The ETOPO1 terrain can be downloaded at https://www.ngdc.noaa.gov/mgg/global/global.html, whereas the ECMWF ERA-Interim reanalysis is available at https://www.ecmwf.int/en/research/climate-reanalysis/era-interim.

References

Alexander, M. J., Geller, M., McLandress, C., Polavarapu, S., Preusse, P., Sassi, F., et al. (2010). Recent developments in gravity-wave effects in climate models and the global distribution of gravity-wave momentum flux from observations and models. *Quarterly Journal of the Royal Meteorological Society*, *136*, 1103–1124. https://doi.org/10.1002/qj.637

Alexander, S. P., Orr, A., Webster, S., & Murphy, D. J. (2017). Observations and fine-scale model simulations of gravity waves over Davis, East Antarctica (69°S, 78°E). *Journal of Geophysical Research: Atmospheres*, *122*, 7355–7370. https://doi.org/10.1002/2017JD026615

Amante, C., & Eakins, B. W. (2009). ETOPO1 1 arc-minute global relief model: Procedures, data sources and analysis, NOAA technical memorandum NESDIS NGDC-24, National Geophysical Data Center, NOAA. https://doi.org/10.7289/V5C8276M

Bramberger, M., Dörnbrack, A., Bossert, K., Ehard, B., Fritts, D. C., Kaifler, B., et al. (2017). Does strong tropospheric forcing cause large-amplitude mesospheric gravity waves? A DEEPWAVE case study. *Journal of Geophysical Research: Atmospheres*, *122*, 11,422–11,443. https://doi.org/10.1002/2017JD027371

Broad, A. S. (1995). Linear theory of momentum fluxes in 3-D flows with turning of the mean wind with height. *Quarterly Journal of the Royal Meteorological Society*, *121*(528), 1891–1902. https://doi.org/10.1002/qj.49712152806

Broutman, D., Eckermann, S. D., Knight, H., & Ma, J. (2017). A stationary phase solution for mountain waves with application to mesospheric mountain waves generated by Auckland Island. *Journal of Geophysical Research: Atmospheres*, *122*, 699–711. https://doi.org/10.1002/2016JD025699

Butchart, N. (2014). The Brewer-Dobson circulation. *Reviews of Geophysics*, *52*(2), 157–184. https://doi.org/10.1002/2013RG000448

Dee, D. P., Uppala, S. M., Simmons, A. J., Berrisford, P., Poli, P., Kobayashi, S., et al. (2011). The ERA-Interim reanalysis: Configuration and performance of the data assimilation system. *Quarterly Journal of the Royal Meteorological Society*, *137*(656), 553–597. https://doi.org/10.1002/qj.828

Doyle, J. D., & Jiang, Q. (2006). Observations and numerical simulations of mountain waves in the presence of directional wind shear. *Quarterly Journal of the Royal Meteorological Society*, *132*(619), 1877–1905. https://doi.org/10.1256/qj.05.140

Dunkerton, T. J. (1984). Inertia–gravity waves in the stratosphere. *Journal of the Atmospheric Sciences*, *41*(23), 3396–3404. https://doi.org/10.1175/1520-0469(1984)041%3C3396:IWITS%3E2.0.CO;2

Eckermann, S. D., & Preusse, P. (1999). Global measurements of stratospheric mountain waves from space. *Science*, *286*(5444), 1534–1537. https://doi.org/10.1126/science.286.5444.1534

Eckermann, S. D., Ma, J., Wu, D. L., & Broutman, D. (2007). A three-dimensional mountain wave imaged in satellite radiance throughout the stratosphere: Evidence of the effects of directional wind shear. *Quarterly Journal of the Royal Meteorological Society*, *133*(629), 1959–1975. https://doi.org/10.1002/qj.187

Eckermann, S. D., Ma, J., & Broutman, D. (2015). Effects of horizontal geometrical spreading on the parameterization of orographic gravity wave drag. Part I: Numerical transform solutions. *Journal of the Atmospheric Sciences*, *72*(6), 2330–2347. https://doi.org/10.1175/JAS-D-14-0147.1

Eckermann, S. D., Broutman, D., Ma, J., Doyle, J. D., Pautet, P. D., Taylor, M. J., et al. (2016). Dynamics of orographic gravity waves observed in the mesosphere over the Auckland Islands during the Deep Propagating Gravity Wave Experiment (DEEPWAVE). *Journal of the Atmospheric Sciences*, *73*(10), 3855–3876. https://doi.org/10.1175/JAS-D-16-0059.1

Ehard, B., Kaifler, B., Dörnbrack, A., Preusse, P., Eckermann, S. D., Bramberger, M., et al. (2017). Vertical propagation of large-amplitude mountain waves in the vicinity of the polar night jet. *Journal of Geophysical Research: Atmospheres*, *122*, 1423–1436. https://doi.org/10.1002/2016JD025621

Fritts, D. C., & Alexander, M. J. (2003). Gravity wave dynamics and effects in the middle atmosphere. *Reviews of Geophysics*, *41*(1), 1003. https://doi.org/10.1029/2001RG000106

Fritts, D. C., Smith, R. B., Taylor, M. J., Doyle, J. D., Eckermann, S. D., Dörnbrack, A., et al. (2016). The Deep Propagating Gravity Wave Experiment (DEEPWAVE): An airborne and ground based exploration of gravity wave propagation and effects from their sources throughout the lower and middle atmosphere. *Bulletin of the American Meteorological Society*, *97*(3), 425–453. https://doi.org/10.1175/BAMS-D-14-00269.1

Guarino, M. V., Teixeira, M. A. C., & Ambaum, M. H. P. (2016). Turbulence generation by mountain wave breaking in flows with directional wind shear. *Quarterly Journal of the Royal Meteorological Society*, *142*(700), 2715–2726. https://doi.org/10.1002/qj.2862

Holton, J. R. (1983). The influence of gravity wave breaking on the general circulation of the middle atmosphere. *Journal of the Atmospheric Sciences*, *40*(10), 2497–2507. https://doi.org/10.1175/1520-0469(1983)040%3C2497:TIOGWB%3E2.0.CO;2

Kaifler, B., Kaifler, N., Ehard, B., Dörnbrack, A., Rapp, M., & Fritts, D. C. (2015). Influences of source conditions on mountain wave penetration into the stratosphere and mesosphere. *Geophysical Research Letters*, *42*, 9488–9494. https://doi.org/10.1002/2015GL066465

Kim, Y. J., Eckermann, S. D., & Chun, H. Y. (2003). An overview of the past, present and future of gravity wave drag parametrization for numerical climate and weather prediction models. *Atmosphere-Ocean*, *41*, 65–98. https://doi.org/10.3137/ao.410105

Klemp, J. B., & Lilly, D. K. (1975). The dynamics of wave induced downslope winds. *Journal of the Atmospheric Sciences*, *32*(2), 320–339. https://doi.org/10.1175/1520-0469(1975)032%3C0320:TDOWID%3E2.0.CO;2

Klinker, E., & Sardeshmukh, P. D. (1992). The diagnosis of mechanical dissipation in the atmosphere from large-scale balance requirements. *Journal of the Atmospheric Sciences*, *49*(7), 608–627. https://doi.org/10.1175/1520-0469(1992)049%3C0608:TDOMDI%3E2.0.CO;2

Kruse, C. G., Smith, R. B., & Eckermann, S. D. (2016). The mid-latitude lower-stratospheric mountain wave "valve layer". *Journal of the Atmospheric Sciences*, *73*(12), 5081–5100. https://doi.org/10.1175/JAS-D-16-0173.1

Long, D. J., Jackson, D. R., Thuburn, J., & Mathison, C. (2012). Validation of Met Office upper stratospheric and mesospheric analyses. *Quarterly Journal of the Royal Meteorological Society*, *139*(674), 1214–1228. https://doi.org/10.1002/qj.2031

Lott, F., & Miller, M. (1997). A new sub-grid orographic drag parameterization: Its formulation and testing. *Quarterly Journal of the Royal Meteorological Society*, *123*(537), 101–127. https://doi.org/10.1002/qj.49712353704

Martin, A., & Lott, F. (2007). Synoptic responses to mountain gravity waves encountering directional critical levels. *Journal of the Atmospheric Sciences*, *64*(3), 828–848. https://doi.org/10.1175/JAS3873.1

Palmer, T. N., Shutts, G. J., & Swinbank, R. (1986). Alleviation of systematic westerly bias in general circulation and numerical weather prediction models through an orographic gravity wave drag parameterization. *Quarterly Journal of the Royal Meteorological Society*, *112*(474), 1001–1039. https://doi.org/10.1002/qj.49711247406

Phillips, D. S. (1984). Analytical surface pressure and drag for linear hydrostatic flow over three-dimensional elliptical mountains. *Journal of the Atmospheric Sciences*, *41*(6), 1073–1084. https://doi.org/10.1175/1520-0469(1984)041,1073:ASPADF.2.0.CO;2

Pulido, M., & Rodas, C. (2011). A higher-order ray approximation applied to orographic waves: Gaussian beam approximation. *Journal of the Atmospheric Sciences*, *68*(1), 46–60. https://doi.org/10.1175/2010JAS3468.1

Sato, K., Watanabe, S., Kawatani, Y., Tomikawa, Y., Miyazaki, K., & Takahashi, M. (2009). On the origins of gravity waves in the mesosphere. *Geophysical Research Letters*, *36*, L19801. https://doi.org/10.1029/2009GL039908

Shutts, G. (1995). Gravity-wave drag parameterization over complex terrain: The effect of critical-level absorption in directional wind-shear. *Quarterly Journal of the Royal Meteorological Society*, *121*(525), 1005–1021. https://doi.org/10.1002/qj.49712152504

Shutts, G. (1998). Stationary gravity-wave structure in flows with directional wind shear. *Quarterly Journal of the Royal Meteorological Society*, *124*(549), 1421–1442. https://doi.org/10.1002/qj.49712454905

Smith, R. B. (1980). Linear theory of stratified hydrostatic flow past an isolated mountain. *Tellus*, *32*, 348–364.

Smith, R. B., Woods, B. K., Jensen, J., Cooper, W. A., Doyle, J. D., Jiang, Q., & Grubišić, V. (2008). Mountain waves entering the stratosphere. *Journal of the Atmospheric Sciences*, *65*(8), 2543–2562. https://doi.org/10.1175/2007JAS2598.1

Teixeira, M. A. C., & Miranda, P. M. A. (2009). On the momentum fluxes associated with mountain waves in directionally sheared flows. *Journal of the Atmospheric Sciences*, *66*(11), 3419–3433. https://doi.org/10.1175/2009JAS3065.1

Teixeira, M. A. C., & Yu, C. L. (2014). The gravity wave momentum flux in hydrostatic flow with directional shear over elliptical mountains. *European Journal of Mechanics-B/Fluids*, *47*, 16–31. https://doi.org/10.1016/j.euromechflu.2014.02.004

Teixeira, M. A. C., Miranda, P. M. A., & Valente, M. A. (2004). An analytical model of mountain wave drag for wind profiles with shear and curvature. *Journal of the Atmospheric Sciences*, *61*(9), 1040–1054. https://doi.org/10.1175/1520-0469(2004)061,1040:AAMOMW.2.0.CO;2

Teixeira, M. A. C., Miranda, P. M. A., & Argain, J. (2008). Mountain waves in two-layer sheared flows: Critical-layer effects, wave reflection, and drag enhancement. *Journal of the Atmospheric Sciences*, *65*(6), 1912–1926. https://doi.org/10.1175/2007JAS2577.1

Whiteway, J. A., & Duck, T. J. (1996). Evidence for critical level filtering of atmospheric gravity waves. *Geophysical Research Letters*, *23*(2), 145–148. https://doi.org/10.1029/95GL03784

Xu, X., Wang, Y., & Xue, M. (2012). Momentum flux and flux divergence of gravity waves in directional shear flows over three-dimensional mountains. *Journal of the Atmospheric Sciences*, *69*(12), 3733–3744. https://doi.org/10.1175/JAS-D-12-044.1

Xu, X., Xue, M., & Wang, Y. (2013). Gravity wave momentum flux in directional shear flows over three-dimensional mountains: Linear and nonlinear numerical solutions as compared to linear analytical solutions. *Journal of Geophysical Research: Atmospheres*, *118*, 7670–7681. https://doi.org/10.1002/jgrd.50471

Xu, X., Song, J., Wang, Y., & Xue, M. (2017). Quantifying the effect of horizontal propagation of three-dimensional mountain waves on the wave momentum flux using Gaussian beam approximation. *Journal of the Atmospheric Sciences*, *74*(6), 1783–1798. https://doi.org/10.1175/JAS-D-16-0275.1

Xu, X., Wang, Y., Xue, M., & Zhu, K. (2017). Impacts of horizontal propagation of orographic gravity waves on the wave drag in the stratosphere and lower mesosphere. *Journal of Geophysical Research: Atmospheres*, *122*, 11,301–11,312. https://doi.org/10.1002/2017JD027528

Xu, X., Shu, S., & Wang, Y. (2017). Another look on the structure of mountain waves: A spectral perspective. *Atmospheric Research*, *191*, 156–163. https://doi.org/10.1016/j.atmosres.2017.03.015